

Importance of First Cycle Conditions on the Electrochemical Performance of Hard Carbon and Prussian White Based Sodium-Ion Batteries Using Fire Resistant, Fluorine-Free Electrolyte

Alexander Buckel,^[a] C. Aram Hall,*^[b] Le Anh Ma,^[a] L. O. Simon Colbin,^[b] Henrik Eriksson,^[c] Ronnie Mogensen,^[a] and Reza Younesi^[b]

Electrolytes based on sodium bis(oxolato)borate (NaBOB) in organophosphates (trimethyl phosphate and triethyl phosphate (TEP)) have shown promise in sodium-ion batteries when compared to conventional electrolytes in that they are fire resistant, fluorine-free and are of lower toxicity. However, these electrolytes tend to exhibit low initial Coulombic efficiency and high overpotentials. We have here demonstrated that NaBOB in TEP can be used in cells with near-commercial capacity

loadings. Furthermore, we have shown that formation cycle conditions have a significant positive effect on the cell performance in these higher mass loading cells, and that modification of the formation cycle conditions can be used to increase the capacity retention, lower the overpotentials, and as such increase the rate capability. The viability of optimized formation protocols was also demonstrated in scaled up prototype cells.

Introduction

Sodium-ion batteries (SIBs), long publicised as the successor to lithium-ion batteries (LIBs) when extractable Li reserves dwindle,^[1–3] have shown great promise for stationary energy storage.^[4–6] SIBs possess great potential to be cheaper and have higher sustainability compared to LIBs as most proposed SIBs do not contain elements like cobalt, lithium, nickel and copper. They also could provide higher safety as there is no risk of copper dissolution from the negative current collector since copper is replaced by aluminium. However, a common bottleneck in regard to safety in batteries is the liquid electrolyte, which is usually both toxic and flammable.^[7–11]

State of the art LIBs typically rely on electrolyte with LiPF₆ salt and carbonate-based solvents (e.g., diethyl carbonate, dimethyl carbonate, ethyl methyl carbonate) resulting in electrolytes that are both flammable and toxic.^[7,11,12] Importing analogous electrolyte to SIBs (*i.e.*, NaPF₆ in carbonates) means

that SIBs present little to no improvement on LIBs in terms of safety if cells leak or undergo thermal runaway. In an effort to improve electrolyte safety, Colbin *et al.*^[13] proposed an electrolyte for SIBs composed of Na bis(oxolato)borate (NaBOB) in triethyl phosphate (TEP), a relatively low toxicity and flame retarding electrolyte solution. Cells using NaBOB in TEP electrolyte (referred to herein as NaBOB TEP) were shown to have promise in low mass loading full-cells using Prussian white cathodes and hard carbon anodes.^[13] These results prompt further study in high mass loading cells, with a critical eye to minimising any negative aspects, like the low initial coulombic efficiencies (ICEs) and high polarisation commonly observed in NaBOB organophosphate electrolytes.^[13–15]

A common approach to improving the performance of cells with a given electrolyte is to use additives to target electrolyte weaknesses,^[16–20] be it a poor ability to form passivating layers, sensitivity to water etc. There is however much value in refining the formation protocol before resorting to the use of additives. Recently, Kishore *et al.*^[21] showed the potential of a refined formation protocol to extend the cycling life of SIBs using Na[Ni,Mn,Mg,Ti]O₂ cathodes and hard carbon anodes with NaPF₆ in ethylene carbonate and diethyl carbonate electrolyte. By varying the formation cycle conditions, the capacity retention after 150 cycles could be varied between as low as 50% and as high as 90%. In addition, they showed that by changing the formation conditions the duration of formation cycling required to sustain 90% capacity retention at 150 cycles could be reduced from 131 h to 45 h. Sun *et al.*^[22] showed more recently that formation at high current density (2 C) produced comparable performance to formation performed at low current density (C/10) in hard carbon half cells using high concentration NaFSI in ionic liquid electrolyte. This current density increase reduced the time of formation from 100 h down to 2.5 h. A decrease in formation time is typically beneficial from an

[a] A. Buckel, Dr. L. A. Ma, Dr. R. Mogensen
Altris AB
Kungsgatan 70b, 753 18 Uppsala (Sweden)

[b] Dr. C. A. Hall, L. O. S. Colbin, Prof. R. Younesi
Department of Chemistry-Ångström Laboratory
Uppsala University
Lägerhyddsvägen 1, Box 538, SE-75121 Uppsala (Sweden)
E-mail: charlesaram.hall@kemi.uu.se

[c] H. Eriksson
LiFeSiZE AB
Lefflersgatan 3A, 754 50 Uppsala (Sweden)

 Supporting information for this article is available on the WWW under <https://doi.org/10.1002/batt.202300533>

 © 2023 The Authors. *Batteries & Supercaps* published by Wiley-VCH GmbH. This is an open access article under the terms of the Creative Commons Attribution License, which permits use, distribution and reproduction in any medium, provided the original work is properly cited.

economical perspective, assuming that the decrease is not achieved through costly alternatives like expensive additives. For example, it was estimated by Wood *et al.*^[23] in their baseline case analysis that wetting and formation cycling accounted for ~6% of the cost per kWh for the cells they studied, and they further estimated that this cost could be reduced by >60% by modifying the wetting and formation procedure.

Herein, we show the effect that formation cycling has on battery cells containing NaBOB TEP with Prussian white and hard carbon electrodes with near-commercial capacity loadings. The effect that current density and temperature of formation on cell performance (principally ICE and solid electrolyte interphase (SEI) properties, cycling lifetime, rate performance and capacity) is presented. In assessing the effects of formation cycling, a range of cell aging mechanisms that are not directly related to formation were seen to overshadow the impact of formation cycling beyond approximately 100 cycles. To characterise and minimise these non-formation related cell aging mechanisms, a range of cell engineering approaches were used. With this understanding, a refined formation protocol is presented for NaBOB TEP electrolyte in full-cell SIBs.

Results and Discussion

Electrochemical characteristics of Prussian white and hard carbon

To evaluate the effects of formation cycling on cell performance, it is necessary to understand the characteristics of the high mass loading Prussian white and hard carbon full cells (loading of 12 mg/cm² for Prussian white and 7 mg/cm² for hard carbon) with NaBOB TEP. Figure 1 shows the first two cycles of a full cell cycled in a 3-electrode configuration. As the full cell is cathode limited, C-rates applied were based on the practical specific capacity of the cathode, 150 mAh/g.^[24] Given

that sodium metal reacts with TEP,^[13] it cannot be used as reference electrode. Instead, partially desodiated Prussian white, discharged to the middle of the upper voltage plateau corresponding to a potential of 3.3 V vs Na⁺/Na, was used as a reference electrode, with the potential adjusted accordingly to Na⁺/Na. Due to a low polarization, flat potential over a wide capacity range and the (electro)chemical compatibility with the system under investigation, this reference electrode was found to be well suited.^[14,25]

In line with previous reports on NaBOB,^[14,15] a sloping plateau starting at a full cell potential of ~1.5 V (or an anode potential of ~1.4 V vs. Na⁺/Na) is evident during the first charge, which is attributed to NaBOB reduction.^[14] Two plateaus are observed in the cathode cycling characteristics in Figure 1(b), due to the two distinct local environments of the Fe. For Fe coordinated with nitrogen (*i.e.*, FeN₆; high-spin iron), Na de/intercalation and the associated Fe(II)/Fe(III) redox occurs at 3.0 V vs. Na⁺/Na. In contrast, Fe coordinated with carbon (*i.e.*, FeC₆; low-spin iron) exhibits this Na de/intercalation and Fe(II)/Fe(III) redox at 3.3 V vs. Na⁺/Na.^[26] During discharging in the lower plateau at 3.0 V vs. Na⁺/Na, the Prussian white also undergoes phase transition from a rhombohedral structure to a cubic structure during desodiation and from the cubic back to rhombohedral structure upon sodiation.^[27] The cycling behaviour of the hard carbon electrode upon sodiation exhibits an initial, steadily decreasing voltage, followed by a plateau-like region at ~0.1 V vs. Na⁺/Na. These domains have been ascribed to Na storage in defect sites and in graphitic layers, and in the nanopores of the hard carbon, respectively.^[28]

Effects of temperature and current on formation cycling

Formation cycling is typically performed at low current rates (*e.g.*, C/10 or C/20),^[29] however any decrease in the duration of formation cycling, for example through an increased current

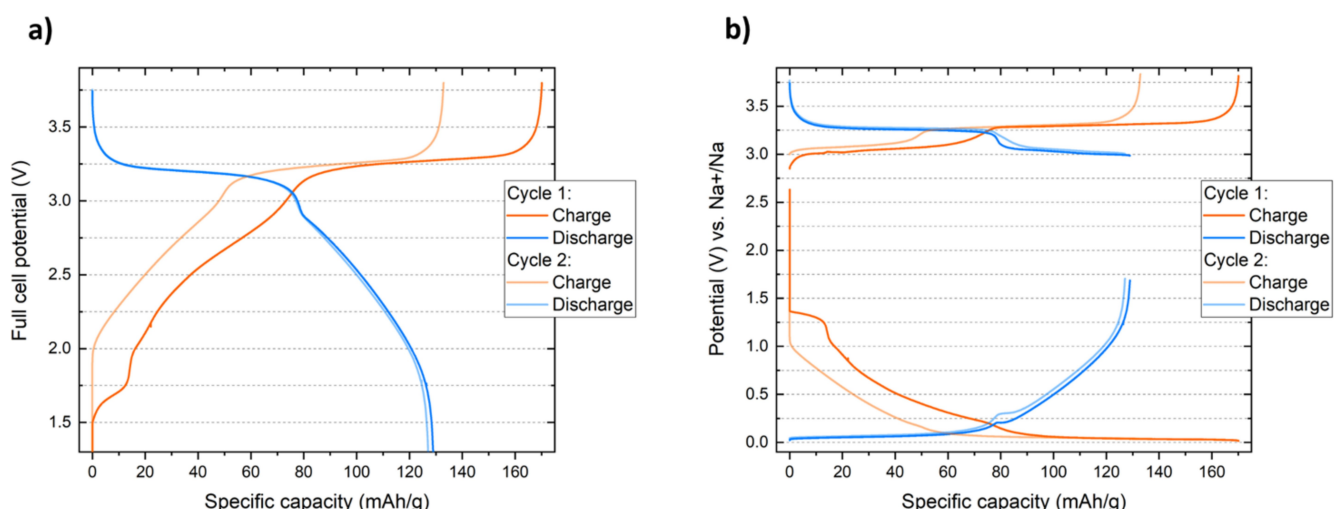


Figure 1. Constant current charge and discharge at C/50 of Prussian white and hard carbon full cells using NaBOB TEP electrolyte in a 3-electrode configuration. Partially desodiated Prussian white at a potential of 3.3 V vs Na⁺/Na was used as the reference electrode, with electrode potentials adjusted so that their potentials are displayed vs Na⁺/Na. The full cell potential in (a) is the potential difference of the electrode potentials shown in (b). The cell was cycled between a full cell potential of 3.8 V and 1.3 V.

density, is advantageous from an industrial perspective.^[21,29] Figure 2 shows the formation protocols assessed in Prussian white hard carbon full cells, along with the cycling parameters.

Initially, the effects of temperature and current density were assessed as the basis for more advanced formation protocol refinement. Cells underwent one of several formation protocols, followed by constant current constant voltage (CCCV) charge at C/5 (CV current threshold set to be equivalent to the current density at C/10) and constant current (CC) discharge at either C/5 or C/2 (beginning with C/5 and alternating every 5 cycles). The increased current rate on discharge was implemented to evaluate the system at higher rates and to reduce cycling time, however an increased current rate was not introduced during charge to avoid premature sodium plating. Formation consisted of one CC charge and discharge, and was performed at either room temperature (21 °C), 30 °C, 50 °C or 70 °C. For each of these formation temperatures, the current density was set at either C/20, C/10 or C/5.

The capacity voltage plots for each of the formation conditions are shown in Figure 3. It is evident from Figure 3 that both temperature and current density during formation affect the charge and discharge capacity. For each of the formation temperatures, a higher current density resulted in a lower charge capacity. Moreover, the difference in this charge capacity between the C/5 and C/20 current density formations is reduced in the cells that underwent formation at higher temperatures. For cells that underwent room temperature, 30 °C or 50 °C formation, the discharge capacity followed a similar trend to charge capacity. However, for cells formed at 70 °C, the trend in discharging capacity was reversed when compared to the charge capacity, with formation at higher current densities producing a greater discharge capacity. It is expected that (electro)chemical reactions are kinetically favoured at higher temperatures and come with a lower overpotential at lower current densities. From the voltage profiles at cycle 1 the capacity attributed to NaBOB decomposition increased at higher temperatures and lower current density. Differences in the magnitude of this decomposition peak are more clearly compared with dQ/dV plots, which are included in the supporting information (see Figure S1).

Aside from RT formation at C/5, discharge capacities were not strongly affected, as shown in Figure 4(a). For Figure 4 and all figures thereafter, cycle 1 refers to the formation cycle and cycle 2 onwards to standard cycling as described by Figure 2. Bazant *et al.*^[30] mentioned charge discharge asymmetry with SEI formation happening primarily during charge, not discharge. With increased charge capacity and similar discharge capacities the trend of decreased Coulombic efficiencies (CEs) follows the expectations as shown in Figure 4(b). The values shown for CE and discharge capacity in Figure 4 are the average of 3 replicates, with the error bars showing the standard deviation of these 3 replicates.

From the CEs of the first 5 cycles after formation, shown in Figure 4(b), it is evident that in all cases the cells are not fully stable after the formation cycle. The comparatively low CEs of the second cycle may suggest that regardless of the formation conditions presented here, thorough passivation requires a subsequent cycle. A close comparison of CEs at 30 °C, 50 °C and 70 °C between cycle 3–6 shows a trend of increased CE with increasing temperature, giving an indication of SEI maturity.

The discharging capacities of the formation cycle and the subsequent 5 cycles are shown in Figure 4(b). It is apparent that for room temperature formation, none of formation protocols presented here are sufficient with all cells dropping well below 100 mAh g⁻¹ within 5 cycles. In contrast, for the cells that underwent formation at elevated temperature, between 120 and 130 mAh g⁻¹ is retained after 5 cycles.

Figure 5 shows the capacity voltage profiles of the 5th cycle. The formation conditions are grouped here with current density in order to make the effect of temperature clearer. There appears to be a visual trend of lower overpotentials in cells formed at higher temperatures. In order to delve further into the effects of the formation conditions on the overpotentials present in the cells, the voltage separation of the upper voltage plateau was used as an estimate. The method for estimating overpotentials was based on the voltage difference between the cell voltage at 75% state of charge during charging and discharging (this process is shown in Figure 5d). This estimation was performed for the 3rd cycle, as in earlier cycles there is evidence from the CEs that the passivation is ongoing, and in later cycles the cells that underwent room temperature

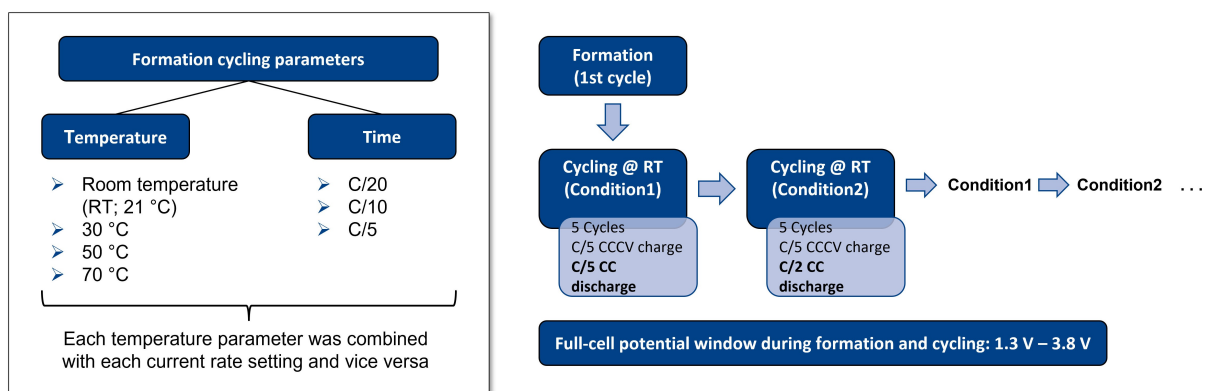


Figure 2. Overview of formation protocols (left) and cycling parameters (right) tested on Prussian white hard carbon full cells.

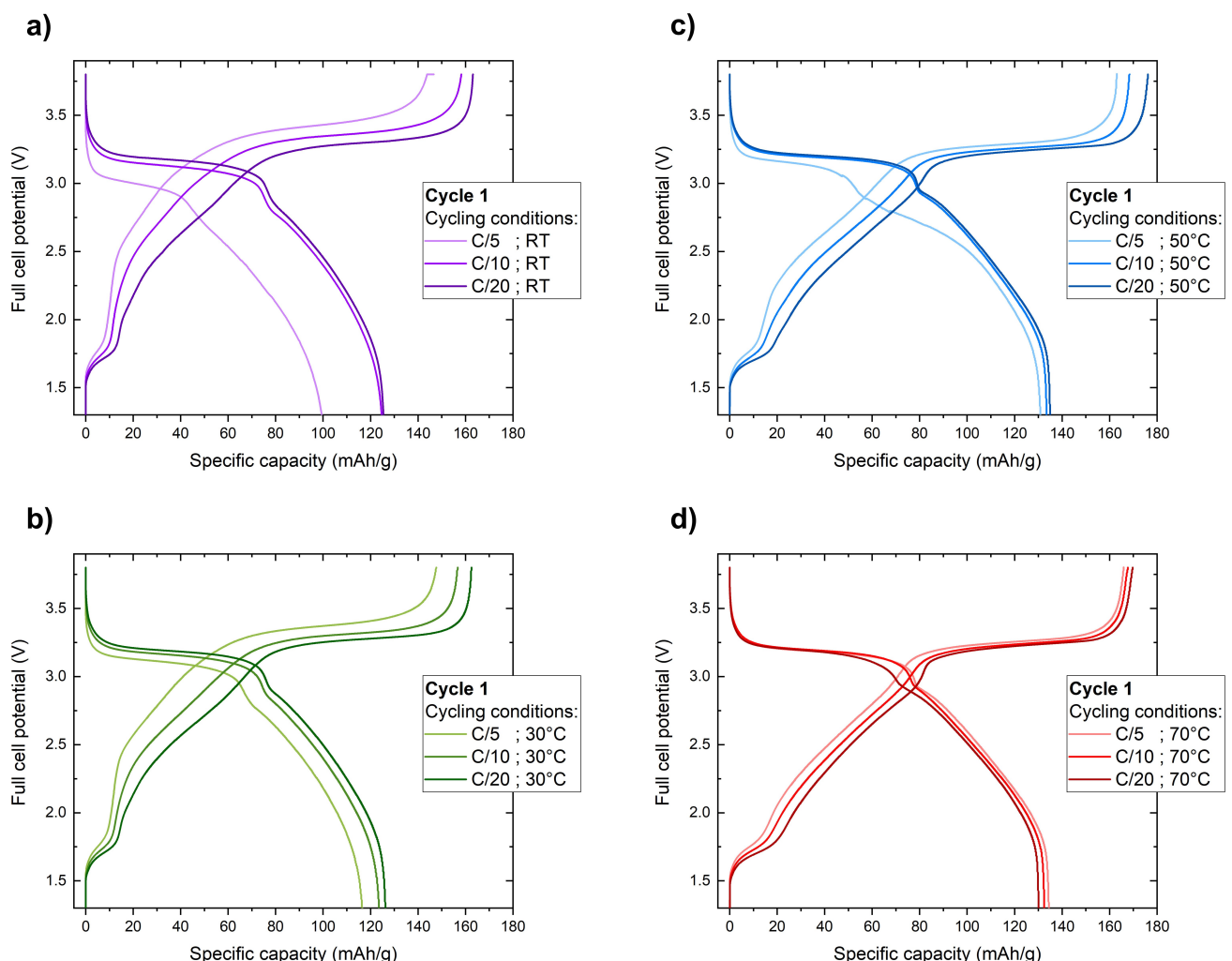


Figure 3. Formation cycle capacity vs. voltage profiles for cells cycled at current rates of C/5, C/10 and C/20. Formation cycles were performed at a) room temperature (21 °C), b) 30 °C, c) 50 °C and d) 70 °C.

formation had begun to degrade significantly. The results of this overpotential estimation are displayed in Figure 5(e).

The estimated overpotentials support the previously stated visual observation that increased temperature of formation reduces the cell overpotential. In contrast, current density variations do not lead to substantial differences, disregarding room temperature cells. Such a conclusion has substantial implications on formation in a commercial setting, with a 75% decrease in formation time (vs. RT C/20 formation) achievable by performing formation at elevated temperatures. It might be that formation time could be even further decreased by going to even higher temperatures, although the extent to which the temperature can be further increased is limited by the cell itself with respect to, e.g., pouch material or separator.

It was expected that differences in cell overpotential would be linked to differences in the SEI. X-ray photoelectron spectroscopy (XPS) on hard carbon electrodes was undertaken after each formation protocol in an effort to link differences in capacity, ICE, and polarization to SEI composition. The relative elemental compositions of the surfaces of discharged hard carbon anodes, following the various formation protocols, is

shown in Figure S2. No discernible trend in the compositional values could be distinguished between post-formation anodes that might explain differences in capacity, ICE or polarization resultant from the differing formation protocols. Due to the relatively minor differences in both the electrochemical and XPS data, it is challenging to clearly identify congruent trends in both measurements. Nonetheless, there is agreement between both techniques in that Coulombic efficiencies from cycle 3–6 are slightly higher for higher formation temperatures while also showing lower overpotentials. Likewise, the XPS results suggest that higher formation temperature reduce substrate related signals (we interpret the intensity, or lack thereof, of the sodiated hard carbon signal in the C1s spectra as an indicator of SEI maturity; see Figure S4 and the accompanying discussion in the Supporting Information), indicating a greater SEI maturity at higher formation temperatures.

Having looked closely at the effects of the formation conditions on the first 5 cycles, longer term cyclability is now considered. The capacity of the first 100 cycles is shown in Figure 6, for which cells were charged under CCCV at C/5, but discharged under CC at either C/5 or C/2, alternating every 5

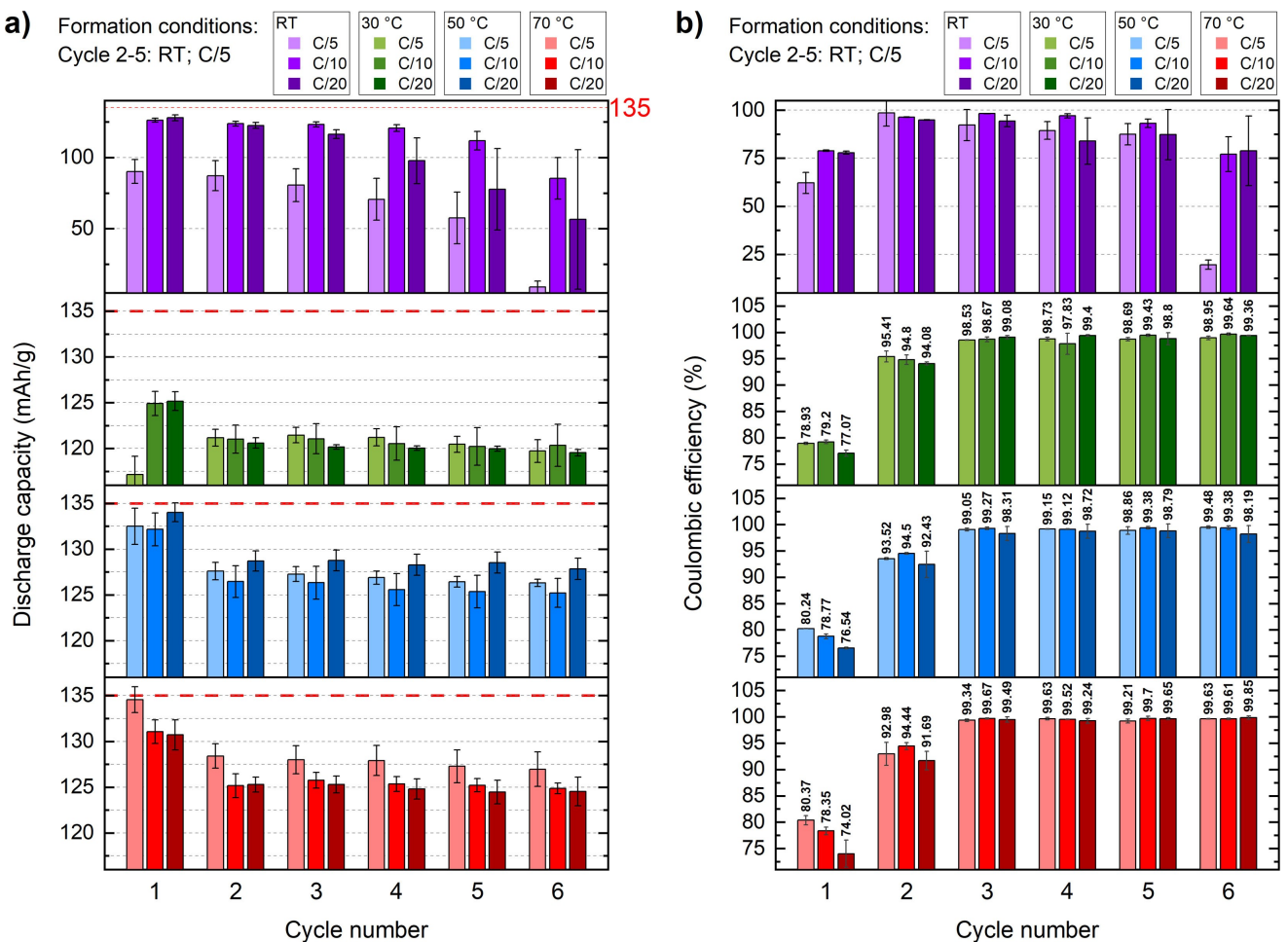


Figure 4. a) Capacity and b) coulombic efficiency over the first 5 galvanostatic charge discharge cycles for cells that underwent formation at current densities of C/5, C/10 and C/20, at temperatures ranging from room temperature (21 °C), 30°C, 50 °C and 70 °C. After the first cycle, the cells were cycled at C/5, with CCCV used for the charge cycle and CC used for the discharge cycle. The discharge capacity and CE values are taken from the average of 3 cells, with the error bars showing the standard deviation from these 3 cells. Note the graph scaling difference in the uppermost section. For ease of comparison, a red line indicating 135 mAh/g was added.

cycles. Significant capacity fade is observed for all cells. Despite the cells that underwent formation at 50 °C achieving higher capacities at the C/5 discharging rate over the first hundred cycles, the cells that underwent formation at 70 °C achieved higher capacities at the C/2 discharging rate. This result agrees with the estimates of the overpotentials provided in Figure 5(e) in so much as higher formation temperature produces lower overpotentials, and as a result would be expected to retain more capacity at higher rates of charge and discharge.

At C/2 discharge the spread in capacity between the samples of nearly 20 mAhg⁻¹ at cycle 7 is reduced to 5 mAhg⁻¹ by the 100th cycle. To investigate the decay mechanisms occurring in the cells, the capacity voltage plots of the second cycle and nearing 100 cycles at C/5 (cycles 5 and 95) and C/2 (cycles 10 and 100) are shown in Figure 6(b). Voltage excursions during charge at cell voltages >3.5 V in the C/5 discharging rate, shown in Figure 6(b), are thought to be at least partially linked to Na plating on the hard carbon anode. Evidence of such plating is apparent in the inset of Figure 6(b), showing an anode after 101 cycles. It should be noted that these voltage

excursions at high potentials were not observed when the cell is discharged at C/2 (Figure 6c). Given that for both C/5 and C/2 discharging the cells are charged at C/5 using CCCV, it is possibly the case that the sodium retained in the anode at the end of the C/2 discharge reduces the barrier to Na intercalation in the subsequent charge cycle. It should also be noted that the voltage excursions observed for C/5 discharge currents may not be entirely attributable to Na plating, and may also arise from other processes, for example, electrolyte oxidation.

Cell engineering and insights into cell aging

Whilst there is evidence that formation cycle conditions have a large effect on the first cycle capacity, the rate capability and the overpotentials, all cells experience almost similar fading over 100 cycles as shown in Figure 6. To compare the formation conditions more thoroughly on extended cyclability, several adjustments to the cell setup have been made to identify and then mitigate the sources of capacity loss unrelated (or not

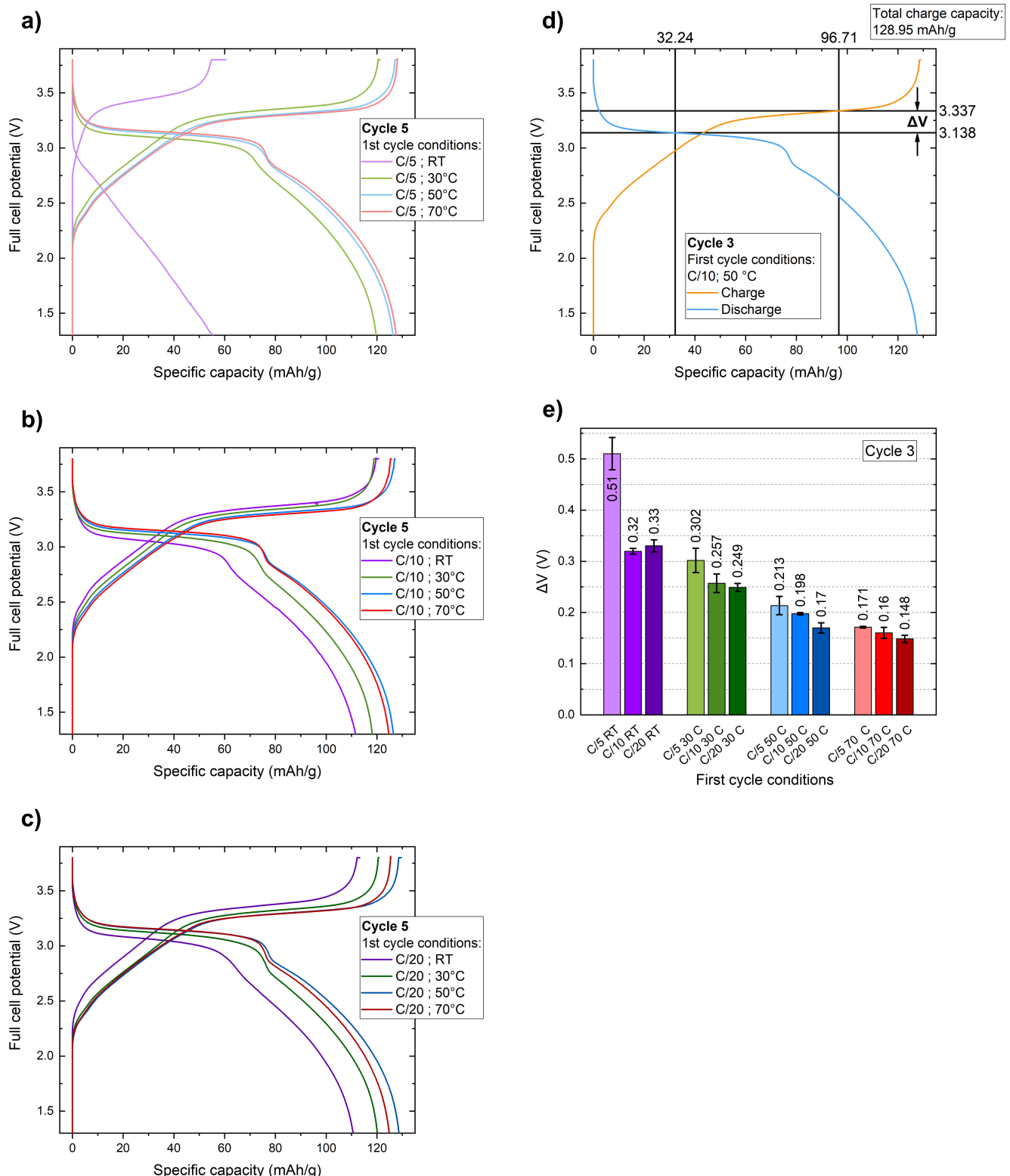


Figure 5. Overpotentials at the 5th cycle resultant from the different formation conditions. The voltage profiles shown in a to c display cycling after formation at a) C/5, b) C/10 and c) C/20. The method used to calculate the overpotentials is shown in (d), with the values for the 3rd cycle shown in (e).

explicitly linked) to formation conditions. For a full discussion of the interventions that have been implemented and their impacts on cycling, the reader is directed to Section 3 of the supporting information.

Considering together the effects of altering the cycling window (Figure S8) and postmortem cell reassembly (Figure S9), it was suspected that much of the capacity loss sprung from the inability of the Prussian white cathode to intercalate Na at

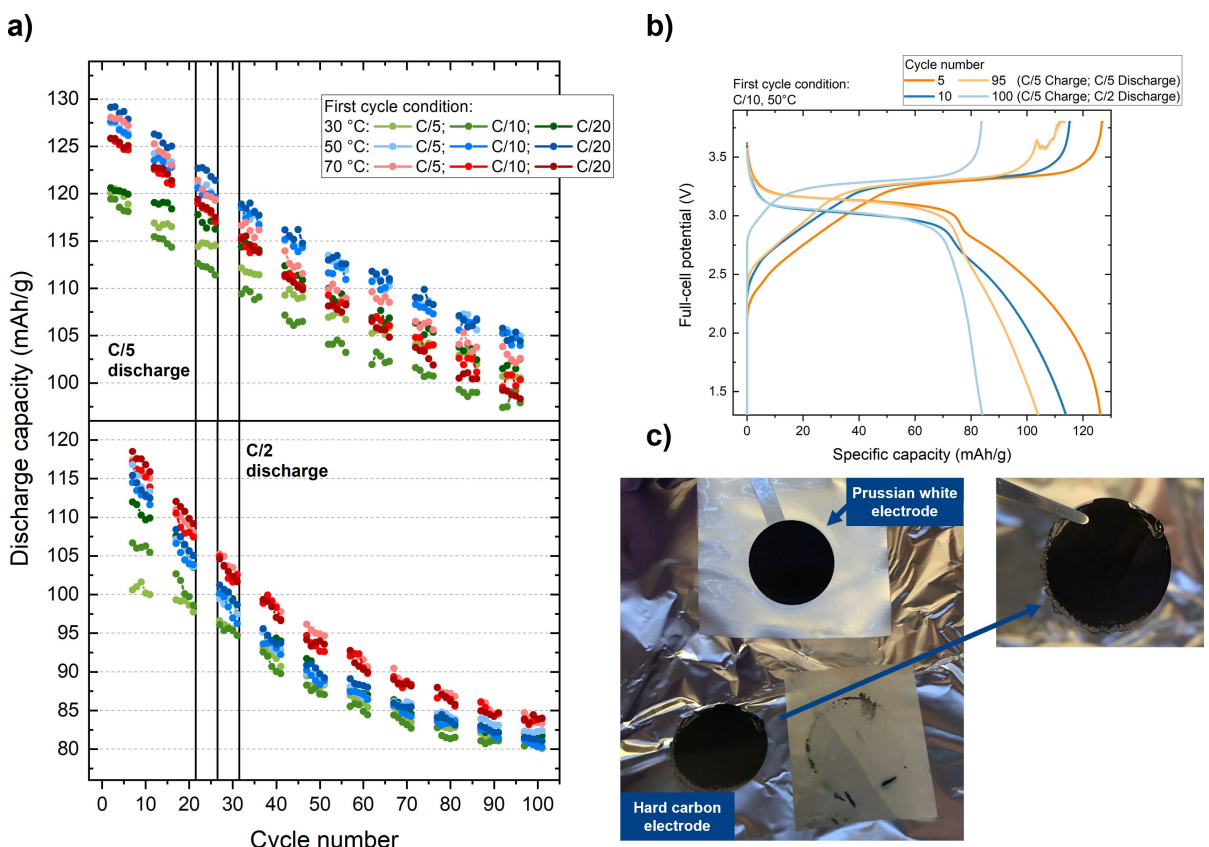


Figure 6. a) Discharge capacities over 100 cycles for current densities alternating between C/5 discharge and C/2 discharge every 5 cycles (C/5 charge in both cases); b) voltage profiles of cycle 5 and 95 (C/5 discharge) and cycle 10 and 100 (C/2 discharge), c) A cell after disassembly showing both fragmentation of, and sodium plating on, the hard carbon anode.

low potentials. Such a result is consistent with the findings of Brant *et al.*^[27] who studied structural changes in Prussian white using operando X-ray diffraction during sodiation and desodiation. They showed that during electrochemical cycling below 3 V vs. Na⁺/Na the crystal structure underwent rearrangement from a cubic structure to a rhombohedral structure. In connection to this, capacity fade was observed in the lower capacity region, as observed here.

Working with the assumption that the phase transition is the root cause of capacity fade, one could conclude that by cycling in voltage regions that avoid these phase transitions, capacity loss could be minimised. To further confirm the same mechanism of capacity fade here, cells were cycled only in the upper voltage regime (2.9–3.5 V), in the lower voltage regime (1.3 V–2.9 V) and as a comparison in the full voltage range (1.3–3.5 V) to minimize or maximize respectively the number of times the Prussian white cathode change from rhombohedral to cubic crystal structure and *vice versa*.

Formation was conducted similarly for all cells, with one cycle at 50 °C between 3.8 V and 1.3 V, followed by room temperature cycling at C/10 for 3 cycles to ensure sufficient SEI maturity. Following this, the cycling window was adjusted to the aforementioned ranges (**upper plateau cycling**: 2.9–3.5 V with CV hold at 3.5 V until $I < C/20$; **lower plateau cycling**: 1.3–2.9 V without CV hold; **full potential region**: 1.3–3.5 V with CV

hold at 3.5 V until $I < C/20$). The cycling results are shown in Figure 7.

Of note, the capacity shown by the cell cycled in the lower capacity region is smaller in absolute terms compared to the capacity shown by the cell cycling in the full potential region below 2.9 V (*i.e.*, for the same voltage region, the cells cycled in the full voltage window show higher capacity). This appears to be due to overpotential during charging of the cell, shown in the full potential region cell as a smeared plateau switch. With this in mind, the upper cutoff potential for the lower plateau cycling could have been adjusted to higher potentials, however it was our intention to remove any low spin Fe contributions. Similarly, the current could have been adjusted to lower rates to reduce the effect of cell overpotential but even then overpotential effects are still observed (see Figure 1).

Over 70 cycles there is no noticeable capacity fade in the cell cycled in the upper voltage regime (0.35% capacity fade from the 5th to the 70th cycle). In contrast cells cycled in the lower voltage regime lose considerable capacity, with 16% of the 5th cycle capacity lost by the 70th cycle. Figure 7(b) plots the capacity voltage curve for a cell cycled with the whole voltage range, with a similar capacity loss analysis in the upper and lower voltage regime. Consistent with the results of the upper and lower voltage cycling, much of the capacity loss in the full

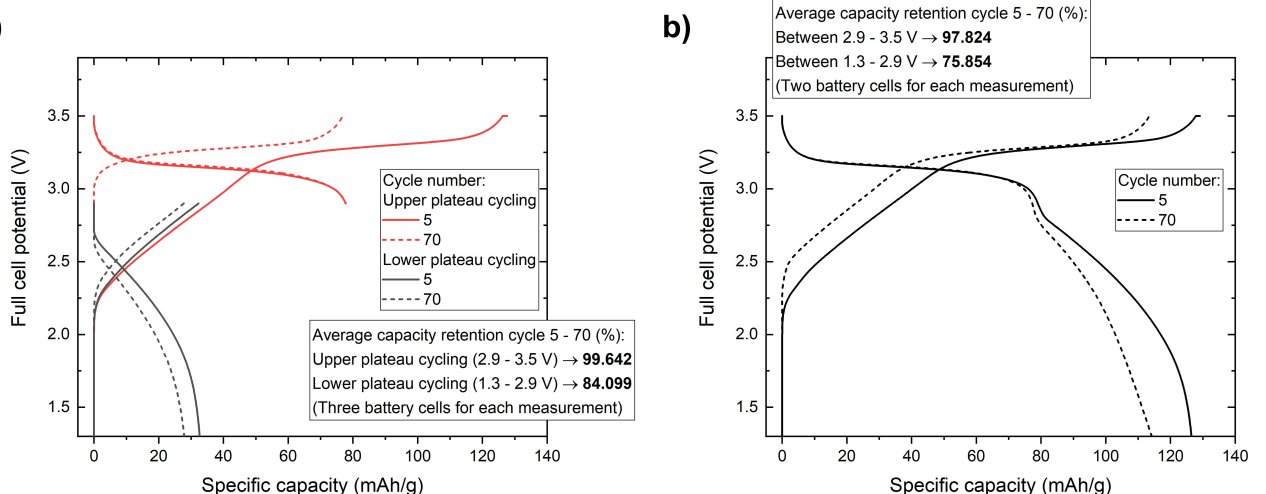


Figure 7. Capacity retention of cells cycled in only the upper plateau (2.9–3.5 V) and lower plateau (1.3–2.9 V) showing: a) the capacity voltage curves of cells cycled in the upper and lower plateau regions at the 5th and 70th cycles; b) the capacity voltage curves of a cell cycled in the full potential region (i.e., 1.3 V to 3.5 V). The capacity retention in the inset of a) is calculated from the capacity of the discharge, whereas in b) it is calculated from the discharge capacity in the 2.9–3.5 V and 1.3–2.9 V portion of the curve.

cell cycling come from the capacity below 2.9 V (24% capacity loss from cycle 5 to cycle 70).

Considering the results together, there is symmetric capacity fade in the cell cycled in the lower plateau cycling experiment, whereas for the full potential region cycling, more capacity fade is observed the lower the potential. This hints towards phase transition during cycling inducing accelerated capacity fade, accompanied by an overpotential increase in the system. Phase transitioning from cubic to rhombohedral phase when discharging the cell is accompanied by a volume reduction of the Prussian white particles. As the particles shrink, it is conceivable that the electronic pathways are inhibited. Judging from slower cycling yielding high capacities in the lower plateau region, it is apparent that this is observed as a kinetic effect, and is thus a power fade rather than a capacity fade.

Further analysis to identify and prevent the power fading inherent to Prussian white is beyond the scope of this study. Nevertheless, it is apparent that both the cell engineering and electrode mechanics can contribute to capacity fade of the cells. Yet, these issues could obscure the effects of formation cycling.

A first step towards a refined formation protocol

The preceding section aimed to identify and – as far as possible – mitigate capacity fade from processes not directly linked to formation cycle conditions. With greater knowledge of the causes of irreversible capacity, we now return to formation cycling conditions. As a final refinement of the formation conditions, the 50 °C, C/10 formation was used as the base for further optimization.

It is evident that depending on formation temperature and current rate, the initial decomposition of NaBOB (in the voltage

region of ~1.5 V onset potential) varies in the absolute capacities involved. Yet correlation to XPS data and cyclability remained absent.

The electrochemical reactions that take place in this region might not necessarily create an SEI directly. Still, it is possible that these reactions serve as building blocks for SEI creation at lower anode potentials. Generally speaking, decomposition reactions upon first charge of a battery cell should be kept at a minimum and are considered unfavourable if not contributing to SEI build-up. Charge balancing sodium ions would limit the accessible storage capacity. Moreover, reactive by-products remaining in the electrolyte might initiate further parasitic reactions.

If this were true, spending longer time at such potentials that BOB⁻ breakdown continued indefinitely without ever forming a passivating layer on the hard carbon anode would result in even greater irreversible capacity in the first cycle. Conversely, spending less time at voltages below the potential at which a passivation layer is formed should reduce the amount of irreversible capacity in the first cycle. To test this hypothesis, two new formation protocols were tested: i) **Hold**, in which CC at C/10 until 1.7 V (the peak potential of the BOB⁻ breakdown), followed by a 10 h voltage hold at 1.7 V, and then CC at C/10 again until 3.8 V; and ii) **Skip**, in which a high current of 10 C was applied until the cell potential reaches 3 V, followed by CV at 3 V for 1 h, and then C/10 until 3.8 V. Both of these protocols were conducted at 50 °C. These formation protocols are shown in Figure 8, along with the base protocol (C/10 at 50 °C) highlighting cycling time for the formation process. After the formation cycle, the cells were cycled at a constant temperature of 30 °C using C/3 CCCV charge and CC discharge between 1.8–3.6 V.

Figure 9 shows the cycling results for the three aforementioned formation protocols. As predicted, the ICE (Figure 9a) is lower in cells that underwent the Hold formation protocol vs.

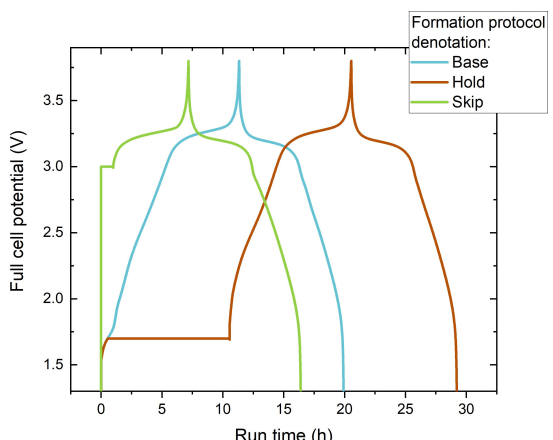


Figure 8. Refined formation cycle protocols showing the **Base**, **Skip** and **Hold** protocols. See the text for a full description of these protocols.

the Base protocol, and higher in cells that underwent the Skip protocol. Consistent with the hypothesis that the attributed BOB⁻ reduction at ~1.5 V onset potential during the first charge does not provide a passivation, the Hold protocol exhibits the largest charge capacity (and also exhibits a measurable (though small) current even after 10 h; see Figure S13), followed by Base and then Skip (Figure 9b). Not only are the ICEs lower for the Hold and Base protocols in comparison to the Skip protocol, the discharge capacities are also lower, again consistent with

the idea that reduction at ~1.5 V onset potential needlessly depletes the sodium inventory.

The second cycle charge capacities match roughly with the discharge capacities of the formation cycle. The second cycle discharge capacity of the cells formed with the Skip protocol is higher by almost 20 mAhg⁻¹ in comparison to cells formed with either the Base or Hold protocols. This capacity surplus is maintained up to 75 cycles.

To further prove the viability and efficacy of the refined Skip protocol, this protocol was implemented in pilot-scale pouch format cells. The cycling results from these pouch cells are shown in Figure 10. A representative cell is shown Figure 10(a), with the modified formation Skip formation protocol shown in Figure S15 and discussed in the accompanying text in the SI.

Based on the results shown in Figure 7(a), whereby capacity fade during cycling was observed to occur when cycling in a 1.3 V to 2.9 V range but not in a 2.9 V to 3.5 V range, cycling of the 4 Ah format pouch cells was split into 2 categories. As a base case, cycling was performed between 1.8–3.5 V, shown in Figure 10(b and d). A second condition was used in which cycling was alternated between 2.7–3.5 V and the full 1.8–3.5 V (alternating 4 cycles of the restricted range and 1 cycle of the full range), shown in Figure 10c and e. The discharge capacity and discharge fading ratio are shown for both of these approaches in Figure 10(b and c), and the cycling profiles at cycles 10, 110, 510 and 950 (i.e., cycles during which both cells were cycled from 1.8–3.5 V) are shown in Figure 10(d and e).

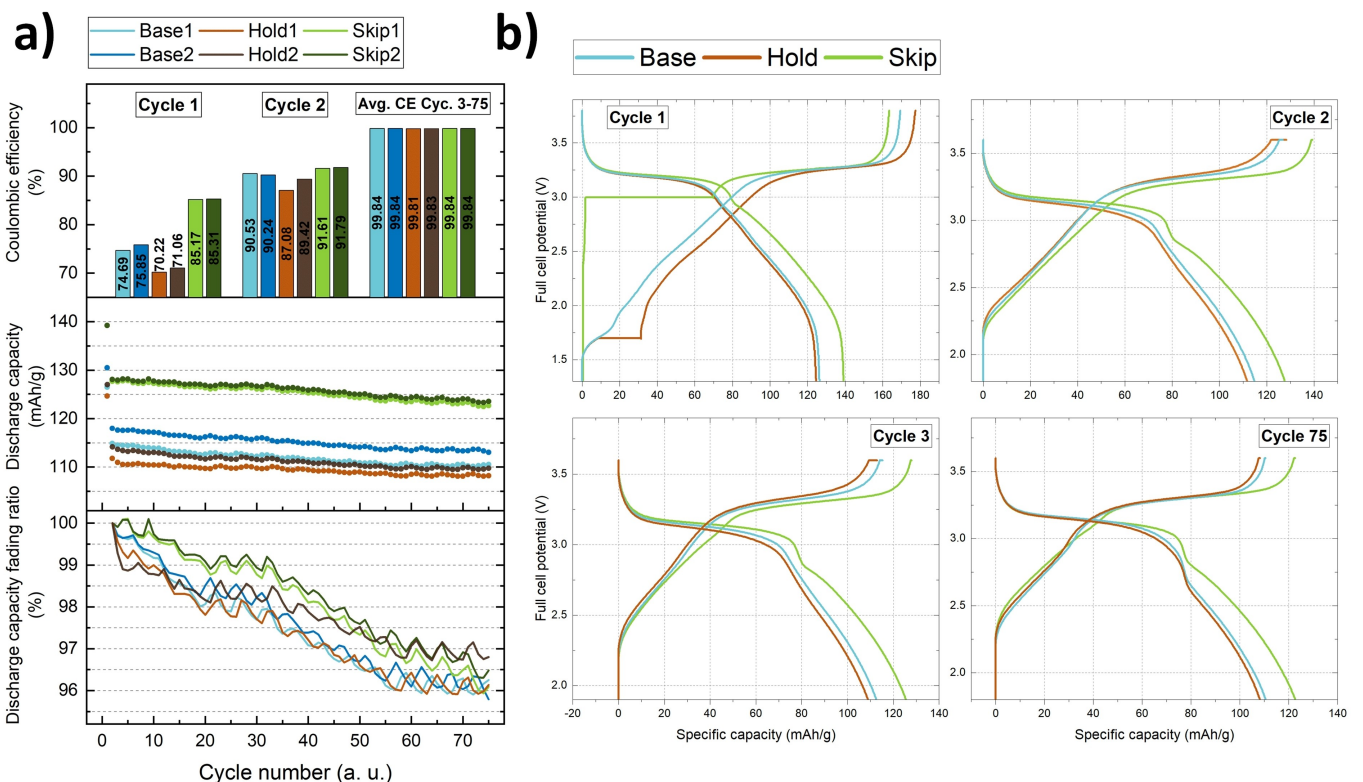


Figure 9. Cycling results of the refined formation protocol showing: a) the CE of the formation cycle (cycle 1), cycle 2 and the average of cycle 3–75 is shown top, with discharge capacity middle and discharge capacity fading ratio bottom, and b) the capacity voltage plots for selected cycles. Replicates are shown in Figure S14.

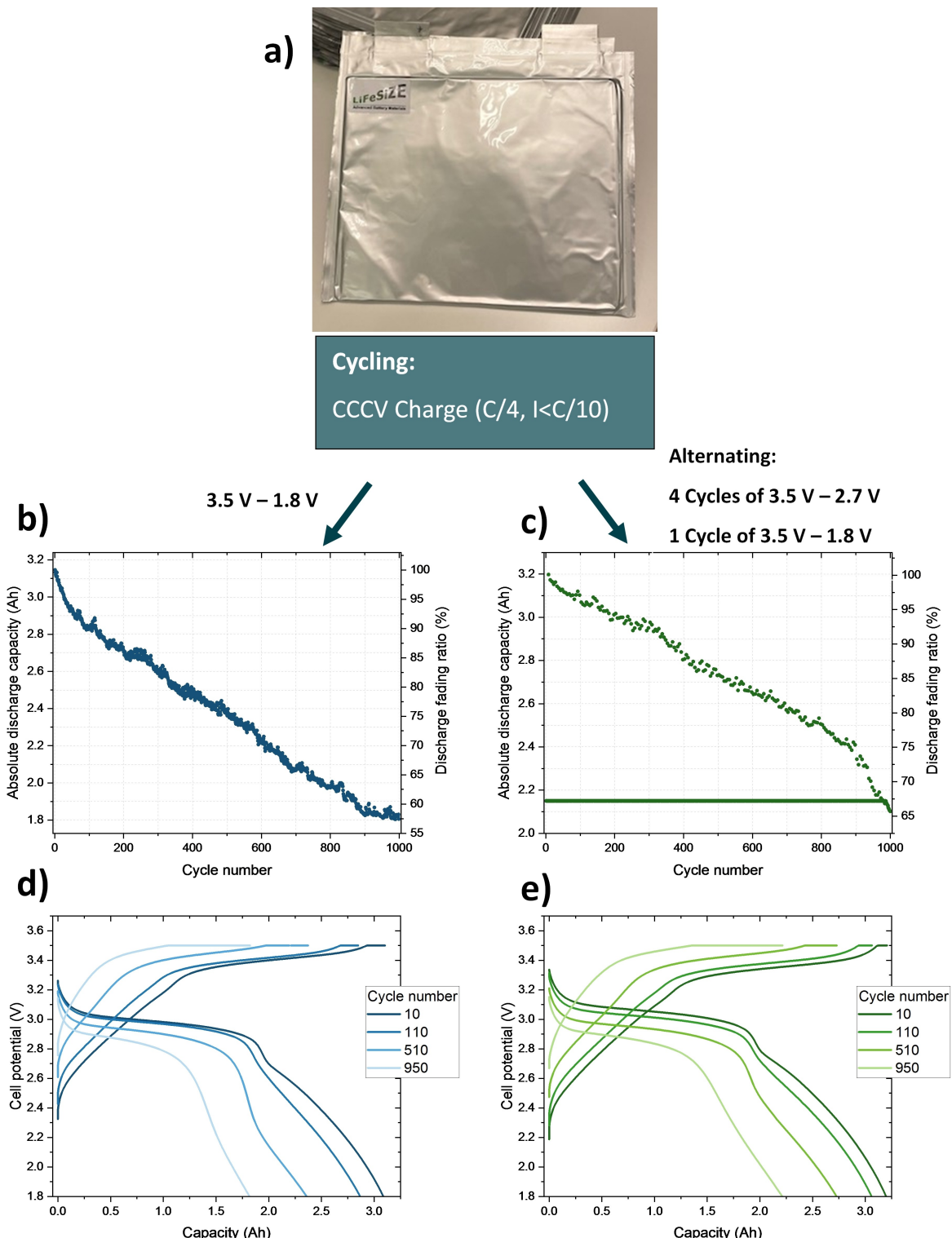


Figure 10. Refined “Skip” formation tested in a 4 Ah format pouch cells. A photo of a representative 4 Ah format cell is shown in a). Two cycling conditions were used whereby cells were cycled in the full 3.5–1.8 V range or in a restricted voltage window (3.5 V to 2.7 V) for 4 cycles followed by 1 cycle of the full 3.5–1.8 V range on a repeating basis. Cyclability and voltage-capacity plots are shown in b and d respectively for the full cycling range. For the alternating restricted and full voltage range, cyclability and voltage-capacity plots are shown in c and e respectively.

When cycling in the full voltage range, the cell is able to cycle to beyond 600 cycles before reaching a 70% discharge fading ratio. For the restricted voltage window, the number of

cycles before reaching a 70% discharge fading ratio is extended even further to ~900 cycles.

Neither cycling under controlled temperature conditions, nor stack pressure has been employed. Particularly the appliance of stack pressure to a system with intrinsic cathode swelling might be beneficial to keep mechanical integrity of the positive electrode intact over extended periods. Besides, due to a jelly-roll configuration with low number of electrode sheets, the high relative excess of anode material yields low initial coulombic efficiencies irrespective of the electrolyte in use. Optimised mixing procedures, electrode recipes, coating procedures, electrode porosities, separator choice, electrolyte loading, use of refined electrolyte formulations and soaking conditions etc. are all well-known to contribute to improved cycling performance. That being said, the results presented here showcase the applicability of NaBOB TEP electrolyte when used in conjunction with refined formation conditions holding promise for Prussian white-, hard carbon-based sodium-ion battery systems to pursue their pathway towards implementation in end-user devices.

Conclusions

We have demonstrated stable long-term cycling of NaBOB TEP electrolyte in cells with near-commercial capacity loadings utilising Prussian white cathodes and hard carbon anodes. To overcome the known issues of thick, resistive SEIs exhibited in cells using NaBOB and organophosphate solvent electrolytes, we have explored the effects that formation cycle conditions have on discharge capacity, ICE and rate capability. Drastic improvement in the performance of cells was achieved by modifying the formation condition from cycling at room temperature with a current density of C/5 to cycling at lower formation currents (C/10 and C/20) at higher formation temperatures (30 °C, 50 °C and 70 °C). The lowest cell overpotential was observed for cells formed with the highest temperature and lowest current (C/20 at 70 °C). Regarding capacity retention, at C/5 discharge, by the 100th cycle the cells formed at 50 °C showed the highest capacity retention; however, consistent with the lower overpotentials observed for cells formed at 70 °C, at C/2 discharge the cells formed at 70 °C exhibited higher capacity retention.

By the 100th cycle, regardless of formation conditions, the capacity of all cells dropped significantly due to processes that we have suggested are more closely linked to aspects of cell engineering than to formation cycle conditions (viz. electrode fragmentation, sodium plating and resistance increase resulting in power fade). This prompted further experiments with restricted voltage windows (either the upper or lower plateau of the Prussian white), which showed that capacity loss seemed to be predominantly linked to a power fade corresponding to the lower voltage plateau of the Prussian white electrode.

After initial modification of the “standard” formation conditions in order to reduce the capacity fading, we have presented a tailored protocol for NaBOB TEP electrolyte. The refined protocol showed substantial improvement to the standard CCCV formation. With this protocol, we have shown 4 Ah multilayer pouch cells using NaBOB TEP electrolyte capable

of cycling to 600 cycles before reaching a discharge fading ratio of 70% (and capable of cycling to beyond 900 cycles before reaching 70% fade when the voltage range is restricted). Hence, formation conditions can be used to overcome the challenges of low ICE, high overpotentials and rapid capacity fade that commonly plague NaBOB in organophosphate electrolytes, and it is speculated that there is further scope for improvement when formation conditions are studied in conjunction with electrolyte additives.

Experimental Section

Electrolyte preparation: NaBOB was synthesised via the Whittingham method^[31] using oxalic acid dihydrate (> 99%, Sigma), boric acid (> 99.5%, Sigma) and sodium hydroxide (> 98%, Alfa Aesar) in a molar ratio of 2:1:1. Having purified the NaBOB via recrystallisation in hot acetonitrile, a further recrystallisation was performed as described by Mogensen *et al.* using trimethyl phosphate.^[14] The NaBOB was dried under vacuum at 100 °C for 48 h inside an Ar filled glovebox. The NaBOB was dissolved in TEP (> 99.8%, Merck) that had been dried over molecular sieves and filtered by a 0.2 µm polypropylene syringe filter (VWR). The electrolyte solution was close to the saturation point of NaBOB with a molal concentration of 0.37.

Cell preparation: Electrodes of Prussian white (Fennac, courtesy of Altris AB) and hard carbon (Kuranode) were produced by LiFeSiZE AB. The slurries were coated onto 15 µm Al foil. Slurries contained the active material with sodium carboxymethyl cellulose and styrene butadiene rubber as a binder. The Prussian white cathodes also contained carbon black as a conductive additive. Mechanical punching of electrodes was conducted with a Hohsen electrode punch and a hammer. Laser cut electrodes were cut with a 532 nm wavelength laser (Östling) with a focal length of 160 mm at 4 W pulsed at 30 kHz. The laser was scanned at 200 mm/s. The hard carbon electrodes were hot calendered (where applicable) to 95% of their initial thickness, whilst the Prussian white electrodes were hot calendered (where applicable) to 90% of their initial thickness.

Pouch cells were assembled in an Ar filled glovebox (O₂ and H₂O < 1 ppm). Prior to assembly, Dreamweaver Gold separators (23 µm) were dried under vacuum at 150 °C for 24 h. Each cell contained 150 µL of electrolyte and was sealed under vacuum. Both the anode and cathode current collector were contacted with strips of Al foil.

Electrochemical Methods: Room temperature cycling was performed with a Neware BTS4000 cycler. Elevated temperature formation was performed with a Novonix cycler in temperature-controlled ovens. Prior to formation, cells were rested for 12 h at the given formation temperature. Current densities were based on the active material mass of the cathode (i.e., excluding the weight of the Al foil, the binder and the carbon black).

Acknowledgements

The authors would like to acknowledge the financial support by the Swedish Energy Agency via project no. 50177-1 and 47523-1, and from the EU project SIMBA (Sodium-Ion and Sodium Metal Batteries for Efficient and Sustainable Next-generation Energy Storage) a European Union H2020 research and innovation programme under Grant agreement No 963542.

Conflict of Interests

The authors declare the following competing financial interest(s): The Prussian white and hard carbon electrodes used in this study were provided by ALTRIS AB, a company founded by R.Y. and R.M. that A.B. is and L.A.M. was employed in. The other authors in this paper declare to have no competing interests.

Data Availability Statement

The data that support the findings of this study are available from the corresponding author upon reasonable request.

Keywords: formation cycling • non-flammable electrolyte • sodium ion battery • Prussian white • hard carbon

- [1] J. Y. Hwang, S. T. Myung, Y. K. Sun, *Chem. Soc. Rev.* **2017**, *46*, 3529.
- [2] P. K. Nayak, L. Yang, W. Brehm, P. Adelhelm, *Angew. Chem. Int. Ed. Engl.* **2018**, *57*, 102.
- [3] M. Baumann, M. Häring, M. Schmidt, L. Schneider, J. F. Peters, W. Bauer, J. R. Binder, M. Weil, *Adv. Energy Mater.* **2022**, *12*, 2202636.
- [4] S. F. Schneider, C. Bauer, P. Novák, E. J. Berg, *Sustain. Energy Fuels* **2019**, *3*, 3061.
- [5] C. Vaalma, D. Buchholz, M. Weil, S. Passerini, *Nat. Rev. Mater.* **2018**, *3*, 1.
- [6] T. Liu, Y. Zhang, Z. Jiang, X. Zeng, J. Ji, Z. Li, X. Gao, M. Sun, Z. Lin, M. Ling, J. Zheng, C. Liang, *Energy Environ. Sci.* **2019**, *12*, 1512.
- [7] Q. Wang, L. Jiang, Y. Yu, J. Sun, *Nano Energy* **2019**, *55*, 93.
- [8] J. Kalhoff, G. G. Eshetu, D. Bresser, S. Passerini, *ChemSusChem* **2015**, *8*, 2154.
- [9] R. Gond, W. van Ekeren, R. Mogensen, A. J. Naylor, R. Younesi, *Mater. Horiz.* **2021**, *8*, 2913.
- [10] Q. Wang, L. Jiang, Y. Yu, J. Sun, *Nano Energy* **2019**, *55*, 93.
- [11] K. Deng, Q. Zeng, D. Wang, Z. Liu, G. Wang, Z. Qiu, Y. Zhang, M. Xiao, Y. Meng, *Energy Storage Mater.* **2020**, *32*, 425.
- [12] N. P. Lebedeva, L. Boon-Brett, *J. Electrochem. Soc.* **2016**, *163*, A821.
- [13] L. O. S. Colbin, R. Mogensen, A. Buckel, Y. L. Wang, A. J. Naylor, J. Kullgren, R. Younesi, *Adv. Mater. Interfaces* **2021**, *8*, 2101135.
- [14] R. Mogensen, S. Colbin, A. S. Menon, E. Björklund, R. Younesi, *ACS Appl. Energ. Mater.* **2020**, *3*, 4974.
- [15] R. Mogensen, A. Buckel, S. Colbin, R. Younesi, *Chem. of Mater.* **2021**, *33*, 1130.
- [16] T. van Ree, *Curr. Opin. Electrochem.* **2020**, *21*, 22.
- [17] H. Zhao, X. Yu, J. Li, B. Li, H. Shao, L. Li, Y. Deng, *J. Mater. Chem. A* **2019**, *7*, 8700.
- [18] N. Xu, J. Shi, G. Liu, X. Yang, J. Zheng, Z. Zhang, Y. Yang, *J. Power Sources Adv.* **2021**, *7*, 100043.
- [19] B. Mosallanejad, S. S. Malek, M. Ershadi, A. A. Daryakenari, Q. Cao, F. Boorboor Ajdari, S. Ramakrishna, *J. Electroanal. Chem.* **2021**, *895*, 115505.
- [20] J. Welch, R. Mogensen, W. van Ekeren, H. Eriksson, A. J. Naylor, R. Younesi, *J. Electrochem. Soc.* **2022**, *169*, 120523.
- [21] B. Kishore, L. Chen, C. E. J. Dancer, E. Kendrick, *Chem. Commun.* **2020**, *56*, 12925.
- [22] J. Sun, I. E. Gunathilaka, L. A. O'Dell, P. C. Howlett, M. Forsyth, *J. Power Sources* **2023**, *554*, 232298.
- [23] D. L. Wood, J. Li, C. Daniel, *J. Power Sources* **2015**, *275*, 234.
- [24] L. Wang, J. Song, R. Qiao, L. A. Wray, M. A. Hossain, Y.-D. Chuang, W. Yang, Y. Lu, D. Evans, J.-J. Lee, S. Vail, X. Zhao, M. Nishijima, S. Kakimoto, J. B. Goodenough, *J. Am. Chem. Soc.* **2015**, *137*, 2548.
- [25] R. Dugas, J. D. Forero-Saboya, A. Ponrouch, *Chem. of Mater.* **2019**, *31*, 8613.
- [26] L. Wang, J. Song, R. Qiao, L. A. Wray, M. A. Hossain, Y.-D. Chuang, W. Yang, Y. Lu, D. Evans, J.-J. Lee, S. Vail, X. Zhao, M. Nishijima, S. Kakimoto, J. B. Goodenough, *J. Am. Chem. Soc.* **2015**, *137*, 2548.
- [27] W. R. Brant, R. Mogensen, S. Colbin, D. O. Ojwang, S. Schmid, L. Häggström, T. Ericsson, A. Jaworski, A. J. Pell, R. Younesi, *Chem. Mater.* **2019**, *31*, 7203.
- [28] M. A. Reddy, M. Helen, A. Groß, M. Fichtner, H. Euchner, *ACS Energy Lett.* **2018**, *3*, 2851.
- [29] D. L. Wood, J. Li, S. J. An, *Joule* **2019**, *3*, 2884.
- [30] P. M. Attia, S. Das, S. J. Harris, M. Z. Bazant, W. C. Chueh, *J. Electrochem. Soc.* **2019**, *166*, E97.
- [31] P. Y. Zavalij, S. Yang, M. S. Whittingham, *Acta Crystallogr. Sect. B* **2003**, *59*, 753.

Manuscript received: November 20, 2023

Revised manuscript received: November 24, 2023

Accepted manuscript online: November 27, 2023

Version of record online: December 13, 2023